



## Sediment control on subduction plate speeds

Behr Whitney M.<sup>a,\*</sup>, Becker Thorsten W.<sup>a,b</sup>

<sup>a</sup> Department of Geological Sciences, Jackson School of Geosciences, University of Texas at Austin, United States of America

<sup>b</sup> Institute for Geophysics, Jackson School of Geosciences, University of Texas at Austin, United States of America



### ARTICLE INFO

#### Article history:

Received 8 May 2018

Received in revised form 29 August 2018

Accepted 31 August 2018

Available online xxxxx

Editor: R. Bendick

#### Keywords:

subduction interface

subduction plate speeds

sediment subduction dynamics

viscous dissipation

deep sediment subduction

India–Asia collision

### ABSTRACT

Tectonic plate velocities predominantly result from a balance between the potential energy change of the subducting slab and viscous dissipation in the mantle, bending lithosphere, and slab–upper plate interface. A range of observations suggest that slabs may be weak, implying a more prominent role for plate interface dissipation than previously thought. The shallow thrust interface is commonly assumed to be weak due to an abundance of fluids and near-lithostatic pore fluid pressures, but little attention has been paid to the influence of the deeper, viscous interface. Here we show that the deep interface viscosity in subduction zones is strongly affected by the relative proportions of sedimentary to mafic rocks that are subducted to depth. Where sediments on the down-going plate are sparse, the deep interface is dominated by mafic lithologies that metamorphose to eclogites, which exhibit viscosities 1–2 orders of magnitude higher than the asthenospheric mantle, and reduce subduction plate speeds. In contrast, where sediments are abundant and subducted to depth, the deep interface viscosity is 1–2 orders of magnitude lower than the asthenospheric mantle, thus allowing significantly faster plate velocities. This correlation between subduction plate speed and deep sediment subduction may help explain dramatic accelerations (or decelerations) in convergence rates, such as the acceleration documented for India–Asia convergence during the mid-Cenozoic.

© 2018 Elsevier B.V. All rights reserved.

### 1. Introduction

Sediment subduction at convergent plate boundaries has long been recognized to play an important role in the dynamics of our planet. Sediments occupying the shallow (seismogenic) subduction interface, for example, appear to influence seismic coupling and the frequency of megathrust earthquakes (e.g. Moore and Saffer, 2001; Heuret et al., 2012), as well as the mechanics and morphologies of accretionary prisms and forearc basins that occupy subduction fronts (e.g. von Huene and Scholl, 1991; Melnick and Echtler, 2006; Simpson, 2010). Sediments subducted to greater depth are essential in the generation of melt, the growth of continental crust, and the cycling of volatiles from Earth's crust and atmosphere to its deep interior (e.g. Hawkesworth et al., 1997; Plank and Langmuir, 1998). Furthermore, because sedimentation patterns are controlled by the distributions of landmasses and their topography, and surface processes such as weathering, erosion, and biologic productivity (themselves sensitive to climate), sediment subduc-

tion represents one of several systems that can exhibit feedbacks between plate tectonics, climate, and life.

Sediment subduction has been suggested to play a particularly important role in weakening or lubrication along the shallow frictional megathrust in modern subduction zones. A range of geophysical, geological and experimental observations suggest that subducted sediments are frictionally weak and/or exhibit high pore fluid pressures (e.g. Kopf and Brown, 2003; Bangs et al., 2009; Tobin and Saffer, 2009). Through their effects on interface shear strength, sediments may control the transmission of stress between the down-going slab and the overriding plate, thus affecting the trench state (advance or retreat), and the upper plate topography and strain regime (von Huene and Scholl, 1991; Clift and Vannucchi, 2004; Beaumont et al., 1999). This sets up interesting potential feedbacks between upper plate uplift patterns and the processes that control sediment supply to the subduction trench. Lamb and Davis (2003), for example, suggested that changes from a sediment-rich to sediment-starved subduction regime during Cenozoic climatic cooling may have been responsible for the rise of the Andean mountain belt. Shorter timescale variations in trench-forearc interactions in the Andes have also been correlated to climate-driven denudation of upper plate topography (Melnick and Echtler, 2006).

\* Corresponding author now at: Geological Institute, Department of Earth Sciences, Swiss Federal Institute of Technology (ETH), Zurich, Switzerland.

E-mail address: [wbehr@ethz.ch](mailto:wbehr@ethz.ch) (W.M. Behr).

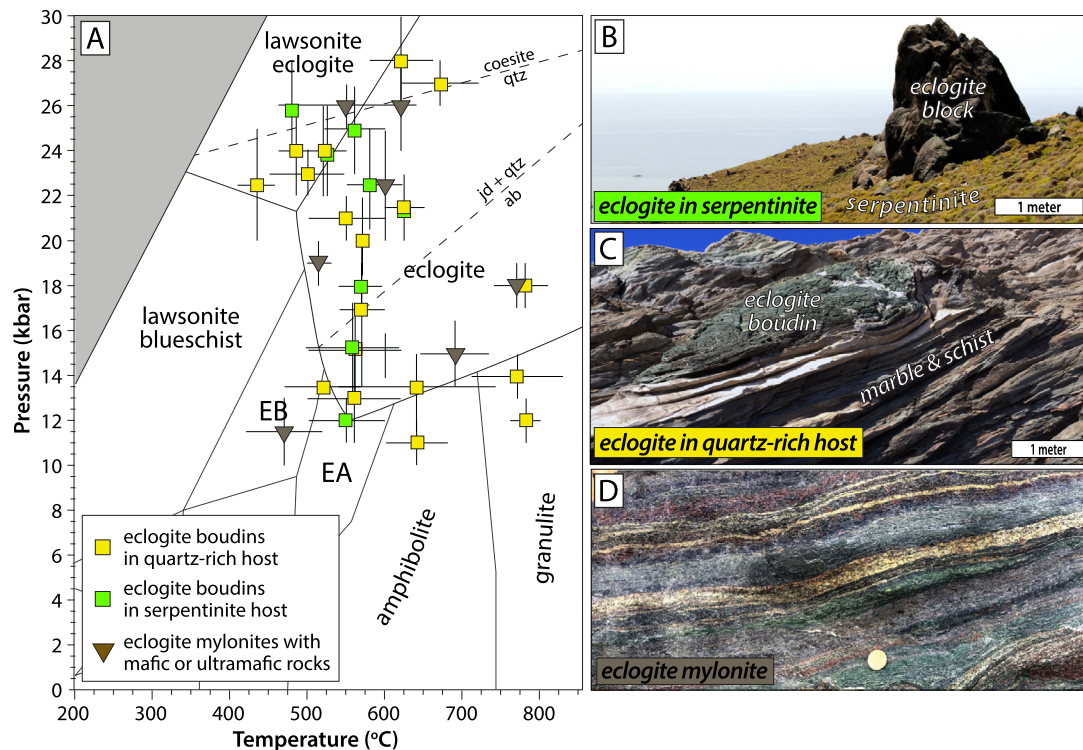


**Fig. 1.** [A] Compilation from the literature of the range of  $P$ – $T$  conditions at which metabasic rocks metamorphosed to eclogite occur in exhumed subduction complexes, color-coded by context/host rock. [B–D] Field photographs of eclogites in the same range of contexts from the Cycladic Blueschist Unit on Syros Island, Greece. (For interpretation of the colors in the figure(s), the reader is referred to the web version of this article.)

A corollary of the role of sediments in lubricating the plate interface is that they should also promote faster subduction speeds. Subducting plate velocities predominantly result from a balance between the potential energy change of the subducting slab, and viscous dissipation in the mantle, bending lithosphere, and slab–upper plate interface. Efforts over the past two decades have focused on quantifying dissipation due to slab bending, originally considered to be one of the largest dissipation sources (e.g. Conrad and Hager, 1999; Becker et al., 1999; Capitanio and Morra, 2012; Garel et al., 2014). By contrast, plate interface dissipation has largely been assumed negligible, partly because of the inference of strong slabs and partly because of the low shear stresses inferred for sediments along the shallow interface (Conrad and Hager, 1999; Duarte et al., 2015). Here we suggest, however, that a reconsideration of the role of the plate interface in controlling plate speeds is warranted for two reasons. Firstly, several recent observations suggest that slabs may in fact be weaker than previously recognized (e.g. Čížková et al., 2002; Wu et al., 2008; Buffett and Becker, 2012; Holt et al., 2015), implying a more prominent role for the plate interface. Secondly, in all subduction zones, the slab–upper plate interface must transition downdip at some depth to a viscous shear zone where rock strength is more sensitive to factors that influence viscosity, such as protolith rock type, temperature, strain rate, water fugacity, and deformation mechanism. This means that even in regions where the shallow frictional interface is weak, resistance to subduction may still be imparted down-dip below the frictional–viscous transition.

In this paper we explore the role of the viscous slab–upper plate interface (herein referred to as the ‘deep plate interface’) in influencing subduction plate speeds. We first use compiled field observations and experimental data to demonstrate that the deep interface viscosity in subduction zones should be strongly affected by the relative proportions of sedimentary to mafic rocks that are subducted to depth. We then evaluate the effects of different interface viscosities on subduction plate speeds for a range of subduc-

tion parameters, including upper plate thickness, and slab strength, age, length, and viscosity. We discuss the implications for modern subduction zones, explore potential feedback mechanisms between sediment subduction and other subduction parameters, and suggest the possibility that subduction of equatorial sediments may have driven the well-documented mid-Cenozoic acceleration of India.

## 2. Viscosity contrast as a function of subducted protolith

Observations from drilling, seismic imaging, and exhumed rocks indicate that the subduction interface can be occupied by a range of rock types derived from mafic oceanic crust, pelagic sedimentary cover, siliciclastic trench fill, and hydrated ultramafic rocks. The most common sedimentary protoliths that occupy the top of subducting slabs in modern subduction zones are argillites and greywackes, silicious oozes and cherts, and pelagic carbonates (e.g. Clift, 2017). With progressive subduction, these protoliths metamorphose to produce schists with variable quartz-mica ratios, meta-cherts, and marbles, respectively. Subducted igneous protoliths derived from the oceanic crust, on the other hand, commonly consist of basalts and gabbros, which metamorphose to form metabasites. In particular, at depths where pressure ( $P$ ) and temperature ( $T$ ) conditions approach  $> 450^\circ\text{C}$  and  $> 12$  kbars, the metabasites dehydrate to form eclogites, which are exceptionally dense rocks composed primarily of omphacitic pyroxene and garnet (Fig. 1). In instances where ultramafic material has been incorporated into the interface shear zone, it is very commonly hydrated to produce serpentinite minerals.

Field observations suggest that these variations in subducted protolith and their metamorphic equivalents result in viscosity variations along the deep subduction interface. Viscosity contrasts between mixed heterogeneous materials can be recognized in outcrop by examining fold wavelengths and boudinage (e.g. Smith, 1977): materials with high viscosity contrast relative to their sur-

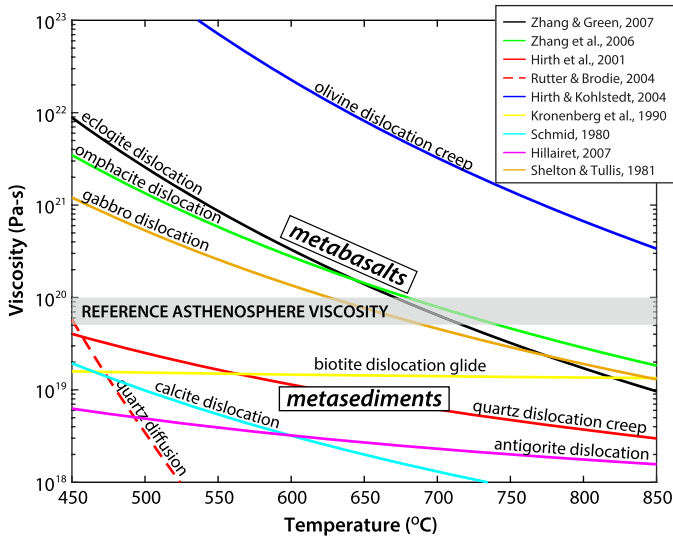


**Fig. 2.** Viscosities as a function of temperature for various rock types derived from rock deformation experiments. Metasediments and serpentinites are predicted to be substantially weaker than the reference asthenospheric mantle viscosity of  $5 \times 10^{19}$ – $1 \times 10^{20}$  Pa s over all deep interface temperatures. Metamafic rocks are predicted to be stronger than asthenospheric mantle over the temperature interval 450–725 °C, but still weaker than the upper plate lithospheric mantle represented by olivine at the same temperature range.

roundings, for example, will commonly occur as massive to weakly deformed lenses, blocks, or boudins embedded in a pervasively sheared matrix. Field data compiled from a range of exhumed subduction complexes demonstrate that metabasites and non-serpentinized ultramafic rocks consistently form blocks or boudins when deformed within metasedimentary or serpentinite host rocks (Fig. 1). These block-in-matrix relationships exist over a wide range of  $P$ – $T$  space, including ultra-high pressure (UHP) conditions characteristic of continental subduction zones. Penetratively deformed or mylonitized eclogites have also been documented over this general  $P$ – $T$  range; these are limited to instances in which eclogite is preserved among other mafic rocks and/or ultramafic peridotites. In these cases, peridotite commonly forms boudins and blocks whereas eclogite composes the weaker host matrix. Thus, the field observations suggest a consistent viscosity hierarchy in which viscosities are lowest in metasediments and serpentinites, higher in eclogites, and highest in peridotites for eclogite-facies conditions characteristic of the deep subduction interface.

The field-based estimates of relative viscosities among different subducted protoliths are also well supported by experimental rock deformation constraints. Fig. 2 shows viscosity as a function of temperature for viscous dislocation creep of the primary strain-accommodating minerals that would be expected to dominate the rheology for different interface rock types (Schmid et al., 1980; Shelton and Tullis, 1981; Kronenberg et al., 1990; Hirth et al., 2001; Hirth and Kohlstedt, 2004; Rutter and Brodie, 2004; Zhang et al., 2006; Zhang and Green, 2007; Hillairiet, 2007). The flow laws are plotted at a strain rate of  $10^{-12}$ /s, which corresponds to a  $\sim 3$  km wide shear zone and a subduction velocity of 10 cm/yr, for example, values reasonable for modern subduction zones. The creep laws indicate that eclogite is up to three orders of magnitude stronger than all metasedimentary and serpentinite rock types. Furthermore, consistent with the qualitative constraints from the field, peridotite is approximately two orders of magnitude more viscous than eclogite over this temperature range. Also plotted for comparison is a reference viscosity for the asthenospheric mantle of  $5 \times 10^{19}$ – $1 \times 10^{20}$  Pa s, which becomes relevant to our analysis in Section 3.

To summarize, both the field and experimental data imply that the viscosity of the deep plate interface should depend strongly on

whether or not sediments are subducted to depth. Where metasediments are subducted to the deep interface, strain will be partitioned into relatively weak minerals such as calcite, quartz, or mica, with viscosities 1–2 orders of magnitude lower than the asthenospheric mantle. Deep sediment subduction will also favor hydration of the mantle wedge to produce serpentinite minerals, also two orders of magnitude weaker than the mantle. By contrast, where metabasic rocks are subducted to depth in the absence of sediments, the degree of serpentinization will be significantly less owing to the much lower volatile content of oceanic crust (e.g. Peacock, 1990), and strain will be partitioned into the higher viscosity eclogite because it is still weak relative to the upper plate lithospheric mantle it is juxtaposed against. These scenarios each represent end-members, but between the sediment-mafic rock endmembers would be shear zones of mixed lithologies with viscosities that are still sensitive to the relative proportions of each rock type (e.g. Handy, 1990).

### 3. Effect of interface viscosity on subduction plate speeds

To explore the potential first order effects of deep interface viscosity contrasts on subducting plate velocities we use a modified version of the semi-empirical formulation for plate velocities presented by Conrad and Hager (1999):

$$V_p = \frac{C_s \rho g \alpha \Delta T l_s h_s - C_f \tau_f l_f}{3\eta_m (A + C_m) + C_l \eta_s (h_s/R)^3} \quad (1)$$

in which plate speed is a balance between a) slab sinking driven by thermal density contrasts, b) dissipation along the slab–upper plate interface, c) dissipation into the convecting mantle, and d) dissipation into the slab itself due to bending (see Table 1 for parameter definitions and values) (Fig. 3). Since we are primarily interested in the role of the viscous plate interface, we recast this equation in terms of viscosity and shear zone width through the relationships  $\eta_f = \tau_f/2\dot{\epsilon}$  and  $\dot{\epsilon} = \delta V_p/2\delta w$ .

To compute the thermal buoyancy of the subducting slab for varying plate lengths, we assume that subducting plate thickness ( $h_s$ ) scales with plate age ( $t$ ) as:  $h_s = 2\sqrt{\kappa t}$ . Dissipation into the subducting slab is related to the slab viscosity ( $\eta_s$ ), its thickness ( $h$ ), and its radius of curvature,  $R$ . Holt et al. (2015) suggest a relationship in which the radius of curvature is approximately linearly correlated with overriding plate thickness such that  $R \approx 1.2h_u + 118$  km, which we utilize here. Dissipation in the mantle surrounding the slab is primarily a function of mantle viscosity ( $\eta_m$ ), which we assume to be  $\sim 10^{20}$  Pa s. Dissipation in the interface shear zone is related to interface viscosity ( $\eta_m$ ) (cf. Fig. 2), the width of the shear zone ( $\delta w$ ), and the length of the shear zone ( $l_f$ ) over which a significant positive viscosity contrast relative to the reference mantle may exist. This length depends on several factors, including the following.

1. The extent to which the interface is dominated by metabasaltic versus metasedimentary rocks. In subsequent plots we express this as a percentage of sediment subducted to depth (specifically, the length of the plate interface that hosts sediments divided by the total length of the interface).
2. The temperature at which metamafic rocks metamorphose to eclogite. We associate this with the blueschist to eclogite transition ( $\sim 450$  °C), which is largely pressure independent for modern subduction thermal gradients (Fig. 1).
3. The maximum temperature at which eclogite exhibits a significant viscosity contrast relative to the reference mantle. We use Fig. 2 to approximate this temperature as  $\sim 725$  °C for a reference mantle viscosity of  $5 \times 10^{19}$ – $1 \times 10^{20}$  Pa s.
4. Geothermal gradient along the plate interface. We relate the interface geothermal gradient to the slab geotherm based on

**Table 1**  
Parameter definitions and value ranges used in plate velocity calculations.

Symbol	Definition	Values	Notes/Source
<b>Slab</b>			
$\theta$	Slab dip	45°	
$\kappa$	Slab thermal diffusivity	10 <sup>-6</sup> m <sup>2</sup> /s	
$t_s$	Slab age	20–150 Ma	
$l_s$	Slab length	50–750 km	
$h_s$	Slab thickness	Scales with $t_s, \kappa$	
$\Delta T$	Temperature difference along slab	1573 K	
$\eta_s$	Slab viscosity	1–500 $\eta_m$	
$R$	Slab radius of curvature	Scales with $h_u$	Holt et al. (2015)
$V_p$	Plate velocity	Solved for	Eq. (1)
<b>Mantle</b>			
$\eta_m$	Mantle viscosity	10 <sup>20</sup> Pa s	
$\rho$	Reference density	3300 g/km <sup>3</sup>	
$A$	Aspect ratio of convecting cell	1.25	Conrad and Hager (1999)
<b>Interface</b>			
$\eta_{sz}$	Shear zone viscosity	1–100 $\eta_m$	cf. Fig. 2
$l_f$	Length of viscous interface	Scales with $\theta, E\Delta T, h_u, t_c$	
$\delta_w$	Shear zone width	2–10 km	
$Ec\Delta T$	$T$ range of potential viscosity contrast	450–725 °C	cf. Fig. 2
<b>Upper Plate</b>			
$h_u$	Upper Plate Thickness	20–150 km	
<b>Constants</b>			
$C_s, C_f, C_m, C_l$	Fitting parameters	1.2, 1, 2.5, 2.5	Conrad and Hager (1999)

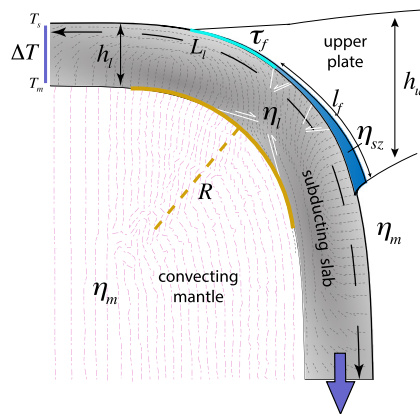


**Fig. 3.** Schematic sketch of the parameters that control the energy balance and associated subduction plate speeds as outlined in Eq. (1). Pink dashed lines in mantle and grey sticks in slab approximate the orientations of the maximum extensional deviatoric stress associated with subduction at this geometry. Modified from Conrad and Hager (1999).

numerical thermal models conducted by Dumitru et al. (1991). Because the geothermal gradient is itself dependent on convergence velocity, we iterate the calculations until the velocity and thermal gradient achieve a steady state.

5. The slab dip angle.
6. The thickness of the upper plate lithosphere. We assume that only the upper plate imparts a viscous resistance to the down-going slab, whereas no resistance is imparted by the mantle wedge.

Within these constraints we solved Eq. (1) for the parameter ranges provided in Table 1.

#### 4. Results

In Fig. 4 we illustrate the variability in the length of the viscous interface ( $l_f$ ) as a function of upper plate thickness and plate age, for a slab dip of 30°, and a viscosity contrast temperature range of

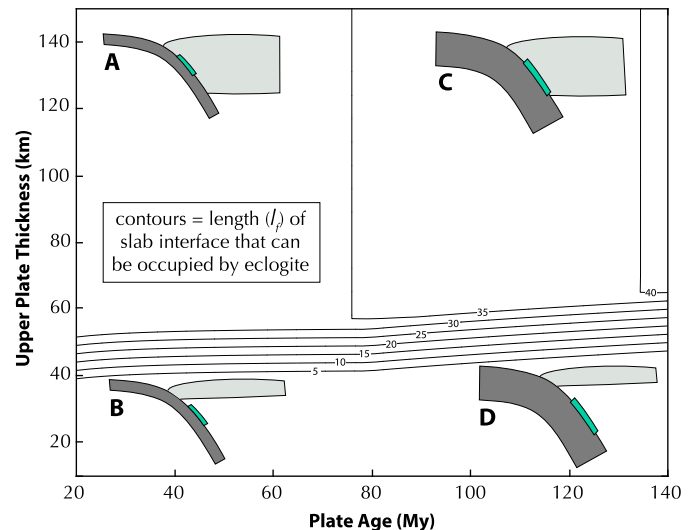


**Fig. 4.** Length of slab interface that can be occupied by high-viscosity eclogite for different upper plate thicknesses and subducting plate ages, plotted for a slab dip of 30°. For cold slabs, the interface geothermal gradient is cooler, so high viscosity eclogite occupies a more extensive region of the slab interface (e.g. sketches C and D), than for younger, warmer slabs (A and B). If the upper plate is thin, however, high viscosity eclogite does not form until the slab has descended into the convecting mantle so does not effect interface coupling (B and D).

450–725 °C. For any combination of these parameters within the ranges given in Table 1,  $l_f$  is largest for subduction zones with thick upper plates (i.e. oceanic–continental) and cold, old, down-going slabs. On the other hand,  $l_f$  is negligible for subduction zones with upper plates thinner than 40 km because in these cases metamafic rocks do not metamorphose to eclogite until well below the slab–upper plate interface.

Fig. 5 shows the effects of interface shear zone viscosity on plate velocity for fixed upper plate thickness, slab viscosity, slab length, and plate age, and for varying interface shear zone widths. The vertical scale of these curves is most sensitive to the main driving force for subduction, which is a function of slab length and

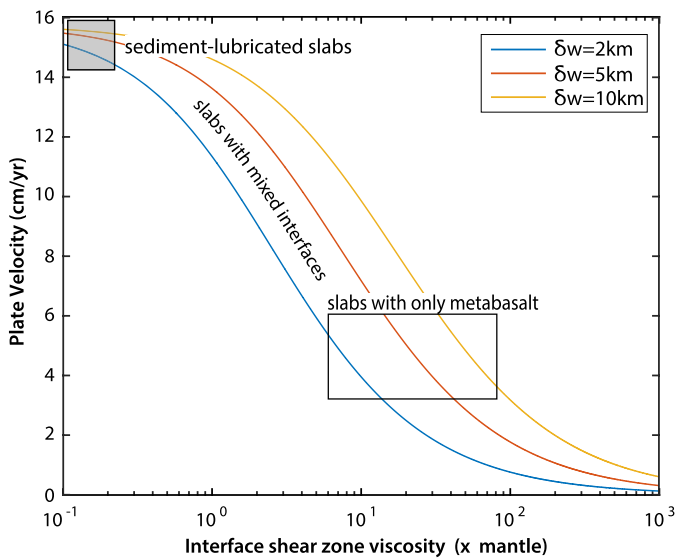


**Fig. 5.** Velocity as a function of interface viscosity for a range of interface shear zone widths. Because of the higher viscosity associated with metabasites metamorphosed to eclogite, slabs with dominantly mafic rocks along their interface should be substantially slowed relative to slabs lubricated by sediments. Upper plate thickness = 100 km; slab viscosity ( $\times$  mantle) = 250; slab length = 1500 km; plate age = 100 m.y.

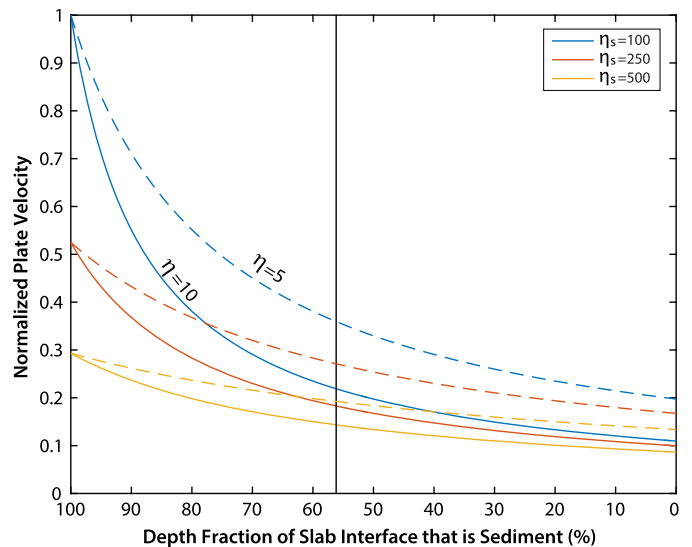
age (i.e. the first term in the numerator of Eq. (1)), whereas the horizontal scale is most sensitive to upper plate thickness and slab strength (in addition to shear zone width, as shown). As based on Fig. 2, metamorphosed sedimentary protoliths are at least one order of magnitude weaker than the asthenospheric mantle over a broad temperature range, so slabs in which sediments fully occupy the viscous interface achieve maximum convergence velocities. Interfaces dominated by serpentinite are expected to behave similarly because of their similarly low viscosity (Fig. 2). By contrast, metabasalts, once metamorphosed to eclogites, exhibit 5–50 times higher viscosities over the temperature range  $\sim 450$ – $725$  °C than the asthenospheric mantle; consequently, plate velocities are predicted to be less than half of the sediment-lubricated plate speed. The narrower the viscous interface shear zone, the more sensitive the plate speeds are to increased viscosity along the interface.

Fig. 6 shows plate velocity (now normalized to the maximum plate velocity) plotted against the depth fraction (in %) of the slab interface that is metasediment for a constant upper plate thickness and plate age, and varying slab strengths and metabasalt viscosities. Similar to what is shown in Fig. 5, the solid and dashed curves illustrate the effect of interface viscosity contrast in affecting plate velocities: for the same sediment-to-mafic-rock ratios, a higher interface viscosity results in a slower plate speed. Furthermore, Fig. 6 shows that the velocities of weak slabs are most sensitive to high viscosity material occupying the interface, whereas the sensitivity of strong slabs is much smaller because strong slabs are already slowed by the energy consumed in slab bending.

## 5. Discussion

### 5.1. Applicability to modern subduction zones

Our calculations show how variations in sediment subduction to the deep interface may influence plate velocities, especially in oceanic–continental subduction zones where the upper plates are relatively thick (cf. Fig. 4). The applicability of these results to modern Earth depend on two main factors: firstly, whether there is significant variability in the amount of sediment subducted to the deep interface; and secondly, whether some slabs are relatively weak (i.e. less than  $\sim 250\times$  the asthenospheric mantle) (cf. Fig. 6).



**Fig. 6.** Normalized plate velocity as a function of the depth % of the slab interface that is occupied by sediment for different slab strengths. Weak slabs are strongly affected by the sediment:metamafic rock ratio along the interface, whereas for strong slabs the effect is small. Black vertical line represents that maximum percent of the interface that can be occupied by eclogite with high viscosity contrast.

*Variations in deep sediment subduction.* The amount of sediment subducted below the forearc is likely to vary significantly, not only from one subduction zone to another, but also within a single subduction zone along-strike and through time (e.g. Shreve and Cloos, 1986; von Huene and Scholl, 1991; Turner and Foden, 2001; Nielsen et al., 2016). Potential causes for variations include differences in sediment supply both along the trench axis and on the deep seafloor, the accretionary vs. erosional state of the subduction zone in the forearc region, and the topography and structure of the down-going slab. Sediment supply near the trench will correlate with proximity to terrestrial landmasses and their topography, whereas sediment supply away from the trench is more sensitive to biologic productivity on the seafloor as a function of climate and latitude (Rea and Ruff, 1996). Accretionary margins will show a greater ratio of subducted sediments to other rock types compared to erosional margins, which have lower sediment supply and also incorporate igneous forearc crust through subduction erosion (von Huene and Scholl, 1991; Clift and Vannucchi, 2004). Seamounts and horsts-and-graben structures will also influence the relative ratios of sediment to metamafic rocks subducted to depth (e.g. Hilde, 1983). Tracers of sediment subduction to the deep interface hosted by arc magmas include cosmogenic  $^{10}\text{Be}$  and a range of trace elements (e.g. Tera et al., 1986; Plank and Langmuir, 1993). Geographic variations in these tracers are very common and indeed suggest different amounts of sediment subduction to the depths of arc magma genesis. Thus, variations in interface viscosity as a function of sediment-to-mafic-rock ratio are likely common in modern earth.

*Mounting evidence for weak slabs.* The second constraint, that some slabs are weaker than  $\sim 250\times$  the surrounding mantle, is also supported by recent observations. The temperature-dependence of viscously deforming mantle rocks alone predicts extremely high viscosities within the cold lithosphere (cf. Fig. 2). However, there are a range of observations that support a relatively modest lithospheric strength, of order 250 times the asthenospheric upper mantle (e.g. Billen, 2008; Becker and Faccenna, 2009). The reason for this apparent reduction in strength is likely that brittle fault-related, and distributed plastic (e.g. Peierl's creep) deformation will serve to weaken the subducting slab within its top and bottom layers, respectively (e.g. Hirth and Kohlstedt, 2004; Mei et al., 2010).

Bending computations and large-scale geodynamic modeling (e.g. Garel et al., 2014; Čížková et al., 2002) indicate the extent of such rheological weakening. For example, a predominantly plastically deforming subducting plate is expected to show a relationship between slab dip and overriding, as opposed to subducting, plate thickness (Buffett and Becker, 2012), and such a relationship is in fact found in nature (Holt et al., 2015). As another example, the recorded post-seismic deformation after the Tohoku-oki 2011 M9 event appears to require weakening of the subducting plate in the depth region where Peierl's plasticity would be expected to operate (Freed et al., 2017). We take these mounting lines of evidence for slab viscosity reduction to be in further strong support for a relatively modest effective viscosity contrast between the slab and mantle of order  $\sim 250$  (cf. Holt et al., 2015).

## 5.2. Feedbacks involving sediment subduction

Our analysis substantiates previous suggestions that sediment subduction (and the numerous processes that control sediment supply to the top of the subducting slab and trench) may profoundly influence the plate-scale dynamics of subduction zones (cf. Lamb and Davis, 2003; Meade and Conrad, 2008; Simpson, 2010). However, despite that theoretical conditions for a sediment-subduction influence on plate speeds appear to be met, we caution that simple correlations between, for example, sediment thicknesses at the trench vs. convergence velocities, are not observed for modern subduction zones globally (Clift and Vannucchi, 2004; Duarte et al., 2015). A direct correlation is not expected, however, partly because the wide range of other variables that influence plate velocity in Table 1 (e.g. slab length, slab age, and upper plate thickness) also vary among and within subduction zones. Furthermore, significant feedbacks between sediment subduction and the other subduction parameters are anticipated, and may skew present-day global correlations.

For example, convergence rate itself may produce a buffering mechanism that prevents runaway plate accelerations. As subducting slabs increase in velocity, their sediment:mafic rock ratios should decrease due to both incorporation of upper plate crystalline crust during subduction erosion and due to the lack of time available for sediments to accumulate in the trench (cf. Clift and Vannucchi, 2004). Additionally, fast convergence results in colder geothermal gradients and therefore greater interface lengths that can be occupied by high viscosity material. Greater interface lengths and lower sediment:mafic rock ratio each serve to increase dissipation into the subduction interface and thus eventually slow plate velocities (cf. Figs. 4 and 6). A similar potential feedback arises when considering the development of topography in the subduction zone upper plate. Thickening of the upper plate by orogeny will increase the length of the viscous interface (cf. Fig. 4), adding resistance and slowing subduction speeds; simultaneously, however, higher topography in the upper plate increases sediment supply to the trench, decreasing interface viscosity and thus lubricating the plate for faster subduction. Both of these feedback mechanisms should result in along-strike variations (e.g. Rodríguez-González et al., 2016) and oscillations in convergence rate over time, and could help explain cycles of upper plate contraction and extension that occur over timescales too short to represent large-scale plate reorganizations, but long enough to accommodate variations in sediment supply to the trench (e.g. in the Andes, cf. Meade and Conrad, 2008; Horton, 2018).

Slab strength may also indirectly influence sediment:mafic rock ratios. Horst and graben topography on the down-going slab has been suggested to increase the amount of sediment subducted beneath the forearc (Hilde, 1983). Graben volumes, in turn, are likely controlled by slab strength, with old, cold, slabs exhibiting a greater depth to the frictional-viscous transition and therefore

potentially deeper graben structures. This suggests that the energy (and subduction speed) that is consumed by slab bending in strong slabs can be offset by greater sediment lubrication along the deep interface.

Additional feedback mechanisms likely exist related to plate age and sediment accumulation on the seafloor; sedimentation patterns as a function of landmass distribution, latitude, and climate; correlations between subduction zone orientations and sediment accumulations; and density variations and contributions to slab pull as a function of oceanic crustal thickness. The feedback mechanisms may have also been quite different for subduction zones during early Earth evolution when oceanic crust was thicker and felsic continental crust and associated terrigenous sediments had yet to evolve. Additionally, several potentially important aspects of plate interface behavior are not included in the analysis above. We do not take into account, for example: 1) the component of viscous dissipation that is converted to heat along the interface and its effect on interface viscosity, 2) variations in the strength of the upper plate lithosphere (due to thermal weakening from the magmatic arc, for example) or the mantle wedge, or 3) along-strike variations in sediment lubrication and how different viscosity regions of the interface interact with each other (especially for slabs with considerable horizontal length). Dynamic models aimed at exploring parameter space and estimating the timescales and magnitudes of feedback effects would be a logical next step in fully quantifying the role of sediments in influencing plate speeds.

## 5.3. Sediment subduction and the mid-Cenozoic acceleration of India

Although correlations between sediment subduction and plate velocities are difficult to evaluate directly for modern subduction zones, examining individual subduction systems for correlations over time is more tractable because over long timescales many of the parameters in Table 1 remain constant or change only gradually.

One example of a potentially compelling correlation between sediment subduction and convergence velocities over time relates to the northward migration of India during closure of the Tethys ocean prior to India-Asia collision. Plate reconstructions based on plate circuit calculations indicate that the motion of India relative to Eurasia from the initiation of subduction at  $\sim 120$  Ma hovered at around 5 cm/yr until 80–90 Ma (Molnar and Stock, 2009; Copley et al., 2010; Cande et al., 2010; Cande and Stegman, 2011; van Hinsbergen et al., 2012). At 80–90 Ma, convergence rates appear to accelerate, reaching a peak of 16 cm/yr at  $\sim 60$  Ma before decreasing again to  $\sim 5$  cm/yr by  $\sim 40$  Ma, with  $\sim 55$  Ma interpreted to represent the timing of India-Asia collision. The overall rapid acceleration in convergence rate from  $\sim 80$ –55 Ma has been variably interpreted, with some models suggesting interactions with a plume head (Cande and Stegman, 2011; van Hinsbergen et al., 2011) and others invoking double subduction (Jagoutz et al., 2015).

Independent of previous interpretations, interestingly, plate reconstructions also suggest a correlation between the acceleration in convergence between India and Eurasia and the arrival of Tethys equatorial bulge sediments at the subduction trench. The equatorial bulge represents a zone between  $\sim 5^\circ$ N and  $5^\circ$ S of high pelagic organism productivity and high sediment accumulation rates associated with mixing of upwelling nutrient-rich deep waters along the equator, with warm tropical waters along the equatorial current system (Theyer et al., 1985; Mitchell, 1998). Fig. 7 shows reconstructions of Indian motion from 120 Ma to 45 Ma as based on the global plate reconstructions of Seton et al. (2012). At the start of Tethys subduction, equatorial sediments were accumulating south of the trench; these sediments first reach the trench at  $\sim 95$  Ma and continue to subduct until collision at  $\sim 55$  Ma, peaking over the same interval as the acceleration in velocity of

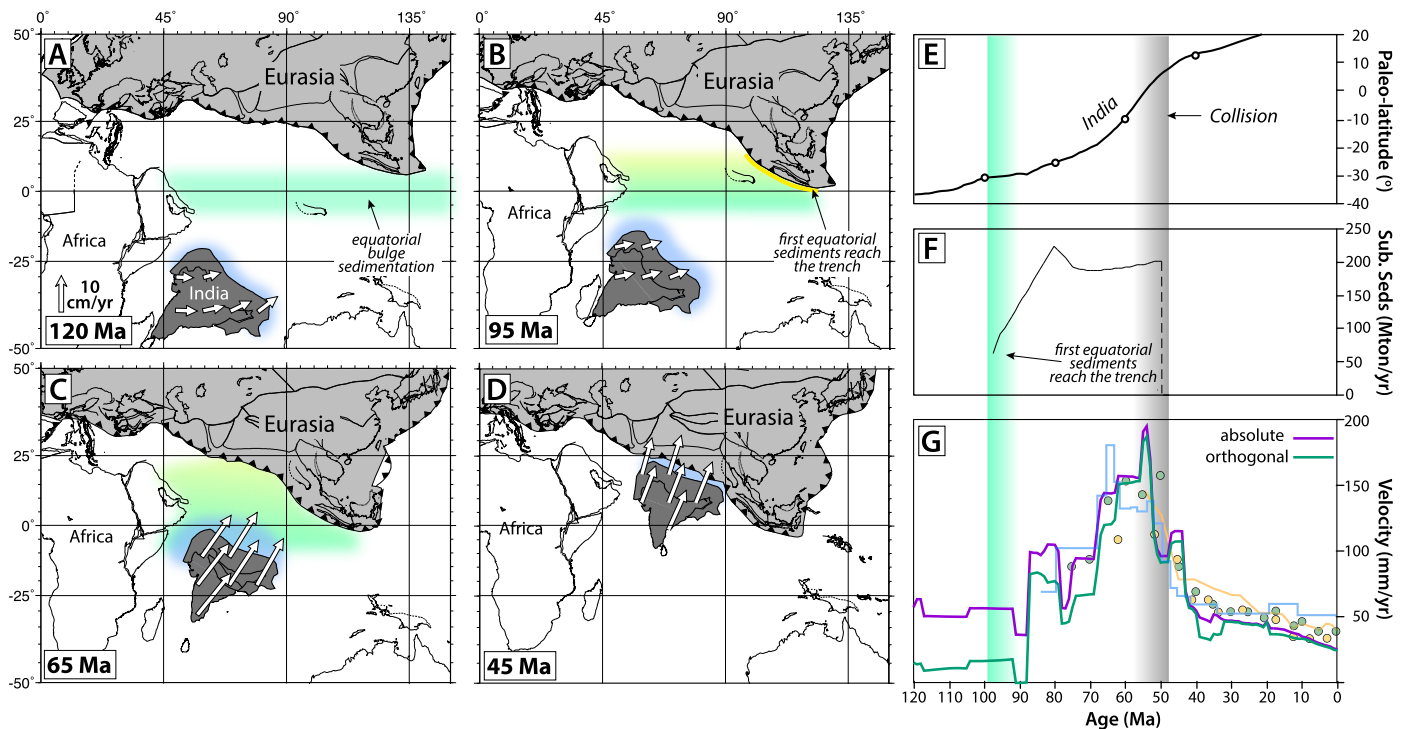


**Fig. 7.** [A–D] Plate reconstructions for India relative to fixed Eurasia from the start of Tethyan subduction at 120 Ma to collision at 45 Ma from Seton et al. (2012). Equatorial bulge sediments (green and yellow) are also tracked as they approach the subduction trench. [E] Paleolatitude of India relative to Eurasia. [F] Estimated amount of subducted sediments from Kent and Muttoni (2013) vs. age for the Tethyan subduction zone. Subduction of equatorial sediments peaks over the same interval as the maximum velocities associated with Indian convergence. [G] Absolute (purple line) and orthogonal (green line) convergence velocity of India relative to Eurasia based on the global reconstructions by Seton et al. (2012). Background points and lines (modified from Jagoutz et al., 2015) includes plate circuit calculations from Molnar and Stock (2009) (light green dots), Copley et al. (2010) (orange dots and orange line), and Cande and Stegman (2011) (blue line).

the Indian plate. The subduction of equatorial pelagic sediments and associated atmospheric  $\text{CO}_2$  from arc volcanoes during closure of the Tethys has in fact been explored as an explanation for Cenozoic Global Warming, which peaked at  $\sim 51$ – $58$  Ma (Kent and Muttoni, 2013; Hoareau et al., 2015). Here we raise the possibility, however, of a causal relationship or positive feedback loop between sediment subduction and convergence rates: equatorial sediment subduction may have induced faster convergence due to deep interface lubrication, which in turn would have driven faster sediment subduction, and so on, until oceanic subduction was terminated when India collided with Asia. This potential mechanism is not incompatible with previous explanations for India's acceleration, but may have acted in concert with plume spreading and/or double subduction (cf. van Hinsbergen et al., 2011; Jagoutz et al., 2015).

## 6. Conclusions

The viscous shear zone within a convergent plate boundary may affect plate speeds as a function of subducted sediment-to-mafic-rock ratio. Sediments are expected to have 2–3 orders of magnitude lower viscosities along the deep interface relative to subducted mafic rocks, which metamorphose to high viscosity eclogite above  $450^\circ\text{C}$ . The velocity-reducing effect of this viscosity contrast is most important for oceanic–continental subduction where the upper plate is relatively thick and if the viscosity of the subducting slab is less than  $250\times$  the asthenospheric mantle. We propose that the mid-Cenozoic acceleration of India's motion during subduction of equatorial pelagic sediments on the Tethys seafloor may at least in part be due to the lubricating effect of sediment subduction. More generally, lithological control of plate boundary strength and hence plate speeds establishes a fundamental link between plate tectonics, climate and life on planet Earth.

## Acknowledgements

This research was funded by NSF CAREER award EAR-1555346 granted to W.M. Behr. W.M. Behr is grateful to Mark Cloos for several informative conversations on topics related to this manuscript. T.W. Becker was partially supported by NSF Geophysics grant EAR-1722680. Both authors thank Adam H. Holt for assistance with the plate reconstructions, and Douwe van Hinsbergen and Simon Lamb for very thoughtful and helpful reviews.

## Appendix A. Supplementary material

Supplementary material related to this article can be found online at <https://doi.org/10.1016/j.epsl.2018.08.057>.

## References

- Bangs, N.L., Moore, G.F., Gulick, S.P., Pangborn, E.M., Tobin, H.J., Kuramoto, S., Taira, A., 2009. Broad, weak regions of the Nankai Megathrust and implications for shallow coseismic slip. *Earth Planet. Sci. Lett.* 284 (1–2), 44–49.
- Beaumont, C., Ellis, S.M., Pfiffner, A., 1999. Dynamics of sediment subduction-accretion at convergent margins: short-term modes, long-term deformation, and tectonic implications. *J. Geophys. Res., Solid Earth* 104 (B8), 17573–17601.
- Becker, T.W., Faccenna, C., 2009. A review of the role of subduction dynamics for regional and global plate motions. In: *Subduction Zone Geodynamics*. Springer, pp. 3–34.
- Becker, T.W., Faccenna, C., O'Connell, R.J., Giardini, D., 1999. The development of slabs in the upper mantle: insights from numerical and laboratory experiments. *J. Geophys. Res., Solid Earth* 104 (B7), 15207–15226.
- Billen, M.I., 2008. Modeling the dynamics of subducting slabs. *Annu. Rev. Earth Planet. Sci.* 36, 325–356.
- Buffett, B., Becker, T., 2012. Bending stress and dissipation in subducted lithosphere. *J. Geophys. Res., Solid Earth* 117 (B5).
- Cande, S.C., Patriat, P., Dymant, J., 2010. Motion between the Indian, Antarctic and African plates in the early Cenozoic. *Geophys. J. Int.* 183 (1), 127–149.

- Cande, S.C., Stegman, D.R., 2011. Indian and African plate motions driven by the push force of the Réunion plume head. *Nature* 475 (7354), 47–52.
- Capitanio, F.A., Morra, G., 2012. The bending mechanics in a dynamic subduction system: constraints from numerical modelling and global compilation analysis. *Tectonophysics* 522–523, 224–234.
- Clift, P., Vannucchi, P., 2004. Controls on tectonic accretion versus erosion in subduction zones: implications for the origin and recycling of the continental crust. *Rev. Geophys.* 42.
- Clift, P.D., 2017. A revised budget for Cenozoic sedimentary carbon subduction.
- Conrad, C.P., Hager, B.H., 1999. Effects of plate bending and fault strength at subduction zones on plate dynamics. *J. Geophys. Res., Solid Earth* 104 (B8), 17551–17571.
- Copley, A., Avouac, J.-P., Royer, J.-Y., 2010. India–Asia collision and the Cenozoic slowdown of the Indian plate: implications for the forces driving plate motions. *J. Geophys. Res.* 115 (B3), B03410.
- Čižková, H., Van Hunen, J., Van den Berg, A.P., Vlaar, N.J., 2002. The influence of rheological weakening and yield stress on the interaction of slabs with the 670 km discontinuity. *Earth Planet. Sci. Lett.* 199 (3–4), 447–457.
- Duarte, J.C., Schellart, W.P., Cruden, A.R., 2015. How weak is the subduction zone interface? *Geophys. Res. Lett.* 42 (8), 2664–2673.
- Dumitru, T.A., Gans, P.B., Foster, D.A., Miller, E.L., 1991. Refrigeration of the western Cordilleran lithosphere during Laramide shallow-angle subduction. *Geology* 19 (11), 1145–1148.
- Freed, A.M., Hashima, A., Becker, T.W., Okaya, D.A., Sato, H., Hatanaka, Y., 2017. Resolving depth-dependent subduction zone viscosity and afterslip from post-seismic displacements following the 2011 Tohoku-oki, Japan earthquake. *Earth Planet. Sci. Lett.* 459, 279–290.
- Garel, F., Goes, S., Davies, D.R., Davies, J.H., Kramer, S.C., Wilson, C.R., 2014. Interaction of subducted slabs with the mantle transition-zone: a regime diagram from 2-D thermo-mechanical models with a mobile trench and an overriding plate. *Geochem. Geophys. Geosyst.* 15 (5), 1739–1765.
- Handy, M.R., 1990. The solid-state flow of polymineralic rocks. *J. Geophys. Res., Solid Earth* 6, 8647–8661.
- Hawkesworth, C.J., Turner, S.P., McDermott, F., Peate, D.W., Van Calsteren, P., 1997. U–Th isotopes in arc magmas: implications for element transfer from the subducted crust. *Science* 276 (5312), 551–555.
- Heuret, A., Conrad, C.P., Funicello, F., Lallemand, S., Sandri, L., 2012. Relation between subduction megathrust earthquakes, trench sediment thickness and upper plate strain. *Geophys. Res. Lett.* 39 (5).
- Hilde, T.W., 1983. Sediment subduction versus accretion around the Pacific. *Tectonophysics* 99 (2–4), 381–397.
- Hirth, G., Kohlstedt, D., 2004. Rheology of the upper mantle and the mantle wedge: a view from the experimentalists. In: *Inside the Subduction Factory*, vol. 138, pp. 83–105.
- Hirth, G., Teyssier, C., Dunlap, W.J., 2001. An evaluation of quartzite flow laws based on comparisons between experimentally and naturally deformed rocks. *Int. J. Earth Sci.* 90 (1), 77–87.
- Hoareau, G., Bomou, B., Van Hinsbergen, D.J.J., Carry, N., Marquer, D., Donnadieu, Y., Le Hir, G., Vrielynck, B., Walter-Simonnet, A.-V., 2015. Did high Neo-Tethys subduction rates contribute to early Cenozoic warming? *Clim. Past* 11, 1751–1767.
- Holt, A.F., Buffett, B.A., Becker, T.W., 2015. Overriding plate thickness control on subducting plate curvature. *Geophys. Res. Lett.* 42 (10), 3802–3810.
- Horton, B.K., 2018. Tectonic regimes of the Central and Southern Andes: responses to variations in plate coupling during subduction. *Tectonics* 37 (2), 402–429.
- Jagoutz, O., Royden, L., Holt, A.F., Becker, T.W., 2015. Anomalously fast convergence of India and Eurasia caused by double subduction. *Nat. Geosci.* 8 (6), 475–478.
- Kent, D.V., Muttoni, G., 2013. Modulation of Late Cretaceous and Cenozoic climate by variable drawdown of atmospheric pCO<sub>2</sub> from weathering of basaltic provinces on continents drifting through the equatorial humid belt. *Clim. Past* 9 (2), 525–546.
- Kopf, A., Brown, K.M., 2003. Friction experiments on saturated sediments and their implications for the stress state of the Nankai and Barbados subduction thrusts. *Mar. Geol.* 202 (3–4), 193–210.
- Lamb, S., Davis, P., 2003. Cenozoic climate change as a possible cause for the rise of the Andes. *Nature* 425 (6960), 792–797.
- Meade, B.J., Conrad, C.P., 2008. Andean growth and the deceleration of South American subduction: time evolution of a coupled orogen-subduction system. *Earth Planet. Sci. Lett.* 275 (1–2), 93–101.
- Mei, S., Suzuki, A., Kohlstedt, D., Dixon, N., Durham, W., 2010. Experimental constraints on the strength of the lithospheric mantle. *J. Geophys. Res., Solid Earth* 115 (B8).
- Melnick, D., Echtler, H.P., 2006. Inversion of forearc basins in south-central Chile caused by rapid glacial age trench fill. *Geology* 34 (9), 709–712.
- Mitchell, N.C., 1998. Modeling Cenozoic sedimentation in the central equatorial Pacific and implications for true polar wander. *J. Geophys. Res., Solid Earth* 103 (B8), 17749–17766.
- Molnar, P., Stock, J.M., 2009. Slowing of India's convergence with Eurasia since 20 Ma and its implications for Tibetan mantle dynamics. *Tectonics* 28, TC3001.
- Moore, J.C., Saffer, D., 2001. Updip limit of the seismogenic zone beneath the accretionary prism of southwest Japan: an effect of diagenetic to low-grade metamorphic processes and increasing effective stress. *Geology* 29 (2), 183–186.
- Nielsen, S.G., Yagodinski, G., Prytulak, J., Plank, T., Kay, S.M., Kay, R.W., Blusztajn, J., Owens, J.D., Auro, M., Kading, T., 2016. Tracking along-arc sediment inputs to the Aleutian arc using thallium isotopes. *Geochim. Cosmochim. Acta* 181, 217–237.
- Peacock, S.A.M., 1990. Fluid processes in subduction zones. *Science* 248 (4953), 329–337.
- Plank, T., Langmuir, C.H., 1993. Tracing trace elements from sediment input to volcanic output at subduction zones. *Nature* 362 (6422), 739–743.
- Plank, T., Langmuir, C.H., 1998. The chemical composition of the subducting sediment and its consequences for the crust and mantle. *Chem. Geol.* 145, 325–394.
- Rea, D.K., Ruff, L.J., 1996. Composition and mass flux of sediment entering the world's subduction zones: implications for global sediment budgets, great earthquakes, and volcanism. *Earth Planet. Sci. Lett.* 140 (1–4), 1–12.
- Rodríguez-González, J., Billen, M.I., Negro, A.M., Montesi, L.G.J., 2016. Along-strike variation in subducting plate velocity induced by along-strike variation in overriding plate structure: insights from 3D numerical models. *J. Geodyn.* 100, 175–183.
- Rutter, E.H., Brodie, K.H., 2004. Experimental grain size-sensitive flow of hot-pressed Brazilian quartz aggregates. *J. Struct. Geol.* 26 (11), 2011–2023.
- Schmid, S.M., Paterson, M.S., Boland, J.N., 1980. High temperature flow and dynamic recrystallization in Carrara marble. *Tectonophysics* 65 (3–4), 245–280.
- Seton, M., Müller, R.D., Zahirovic, S., Gaina, C., Torsvik, T., Shephard, G., Talsma, A., Gurnis, M., Turner, M., Maus, S., Chandler, M., 2012. Global continental and ocean basin reconstructions since 200 Ma. *Earth-Sci. Rev.* 113 (3–4), 212–270.
- Shelton, G.L., Tullis, J., 1981. Experimental flow laws for crustal rocks. *Eos Trans. AGU* 62, 396.
- Shreve, R.L., Cloos, M., 1986. Dynamics of sediment subduction, melange formation, and prism accretion. *J. Geophys. Res., Solid Earth* 91 (B10), 10229–10245.
- Simpson, G.D.H., 2010. Formation of accretionary prisms influenced by sediment subduction and supplied by sediments from adjacent continents. *Geology* 38 (2), 131–134.
- Smith, R.B., 1977. Formation of folds, boudinage, and mullions in non-Newtonian materials. *Bull. Geol. Soc. Am.* 88 (2), 312–320.
- Tera, F., Brown, L., Morris, J., Sacks, I.S., Klein, J., Middleton, R., 1986. Sediment incorporation in island-arc magmas: inferences from <sup>10</sup>Be. *Geochim. Cosmochim. Acta* 50 (4), 535–550.
- Theyer, F., Mayer, L.A., Barron, J.A., Thomas, E., 1985. The equatorial Pacific High-Productivity Belt: elements for a synthesis of Deep Sea Drilling Project Leg 85 results. In: *Initial Reports of the Deep Sea Drilling Project*, vol. 85. U.S. Government Printing Office, Washington, D.C., pp. 971–985.
- Tobin, H.J., Saffer, D.M., 2009. Elevated fluid pressure and extreme mechanical weakness of a plate boundary thrust, Nankai Trough subduction zone. *Geology* 37 (8), 679–682.
- Turner, S., Foden, J., 2001. U, Th and Ra disequilibria, Sr, Nd and Pb isotope and trace element variations in Sunda arc lavas: predominance of a subducted sediment component. *Contrib. Mineral. Petrol.* 142 (1), 43–57.
- van Hinsbergen, D.J.J., Lippert, P.C., Dupont-Nivet, G., McQuarrie, N., Doubrovine, P.V., Spakman, W., Torsvik, T.H., 2012. Greater India Basin hypothesis and a two-stage Cenozoic collision between India and Asia. *Proc. Natl. Acad. Sci. USA* 109 (20), 7659–7664.
- van Hinsbergen, D.J.J., Steinberger, B., Doubrovine, P.V., Gassmöller, R., 2011. Acceleration and deceleration of India–Asia convergence since the Cretaceous: roles of mantle plumes and continental collision. *J. Geophys. Res.* 116 (B6), B06101.
- von Huene, R., Scholl, D.W., 1991. Observations at convergent margins concerning sediment subduction, subduction erosion, and the growth of continental crust. *Rev. Geophys.* 29 (3), 279.
- Wu, B., Conrad, C.P., Heuret, A., Lithgow-Bertelloni, C., Lallemand, S., 2008. Reconciling strong slab pull and weak plate bending: the plate motion constraint on the strength of mantle slabs. *Earth Planet. Sci. Lett.* 272 (1–2), 412–421.
- Zhang, J., Green, H.W., 2007. Experimental investigation of eclogite rheology and its fabrics at high temperature and pressure. *J. Metamorph. Geol.* 25 (2), 97–115.
- Zhang, J., Green II, H., Bozhilov, K., 2006. Rheology of omphacite at high temperature and pressure and significance of its lattice preferred orientations. *Earth Planet. Sci. Lett.* 246 (3–4), 432–443.